Development of a novel emulsified asphalt enhanced steel slag-based geopolymer foamed concrete

Yang, Xinkui; Wu, Shaopeng; Xu, Shi; Chen, Dongyu; Zhao, Zenggang; Chen, Boyu; Liang, Xuhui

DOI
10.1016/j.conbuildmat.2024.139287

Publication date
2024

Document Version
Final published version

Published in
Construction and Building Materials

Citation (APA)
Yang, X., Wu, S., Xu, S., Chen, D., Zhao, Z., Chen, B., & Liang, X. (2024). Development of a novel emulsified asphalt enhanced steel slag-based geopolymer foamed concrete. *Construction and Building Materials*, *456*, Article 139287. https://doi.org/10.1016/j.conbuildmat.2024.139287

Construction and Building Materials 456 (2024) 139287

Contents lists available at ScienceDirect

Construction and Building Materials

journal homepage: www.elsevier.com/locate/conbuildmat

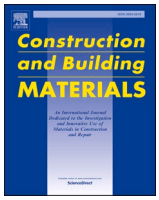

Development of a novel emulsified asphalt enhanced steel slag-based geopolymer foamed concrete

Xinkui Yang [a], Shaopeng Wu [a,*], Shi Xu [b,c,*], Dongyu Chen [a], Zenggang Zhao [a], Boyu Chen [c], Xuhui Liang [c]

[a] State Key Laboratory of Silicate Materials for Architectures, Wuhan University of Technology, Wuhan 430070, China
[b] School of Civil Engineering and Architecture, Wuhan University of Technology, Luoshi Road 122, Wuhan 430070, China
[c] Faculty of Civil Engineering and Geosciences, Delft University of Technology, Stevinweg 1, Delft 2628 CN, the Netherlands

ARTICLE INFO

Keywords:
Geopolymer
Foamed concrete
Steel slag
Emulsified asphalt
Pore structure
Physical properties

ABSTRACT

Steel slag-based geopolymer foamed concrete (SSGFC) provide a promising value-added and carbon-neutral strategy for the re-utilization of SS, and the strength and physical properties of SSGFC are essential to its practical application. Therefore, this study proposes to use emulsified asphalt (EA) to improve the pore structure, compressive strength, water resistance and thermal insulation properties SSGFC. Firstly, different contents of EA were added into the foaming solution to prepare modified foam, and then SSGFC samples were prepared by using modified foam and steel slag-based geopolymer. The fresh properties, microstructure, pore structure, reaction products and physical properties of SSGFC samples were investigated. The results indicate that EA can reduce the fluidity and settlement value of the paste and increase the setting time. The addition of EA leads to a decrease in hydration products, but it can reduce the average pore diameter of the SSGFC and improve its pore diameter distribution. The SSGFC sample prepared by modified foam with 10 % EA showed the best physical properties. Compared with the control group, its compressive strength increased by 21.4 %, water absorption decreased by 16.5 %, and thermal conductivity decreased by 31.3 %. Therefore, EA shows significant potential to enhance the performance of SSGFC, thus providing reliable support for its practical applications.

1. Introduction

As a kind of metallurgical solid waste, steel slag (SS) is generated during the process of iron and steel smelting, formed by solidification of impurities and oxides in molten steel during cooling process [1–4]. In 2022, China's SS total production reached 153 million tons, however, fewer than 30 % of SS is used comprehensively [5–7]. Most SS is still end up with open-air stacking, causing not only wastage of land resources but also heavy metal pollution to the surrounding soil and water. Using SS as precursor to prepare geopolymer provide a promising value-added and carbon-neutral strategy for the re-utilization of SS [8–11]. Shi et al. [12,13] used SS as geopolymer precursor and aggregate to prepare functional composite concrete with excellent mechanical properties and radiation shielding properties. The results show that SS can not only significantly improve the radiation attenuation ability of composite concrete, but also improve the pore structure of composite concrete, thereby enhancing its mechanical properties. However, the inherent constraints in stability and strength pose challenges for the widespread application of steel slag-based geopolymers in functional structures like foamed concrete [14].

Foamed concrete is produced by adding foam into cement paste through physical or chemical methods [15,16]. It has the advantages of light weight, heat insulation, noise reduction, etc., and can be employed to various non-load-bearing structures, such as building insulation layer, road base, bridge deck filling layer, etc. [17–20]. Ordinary Portland cement is the primary material for producing foamed concrete, which involves high-temperature calcination and limestone calcination processes during its production, resulting in significant carbon dioxide (CO_2) emissions, thus exacerbating the greenhouse effect [21,22].

Geopolymer is a kind of aluminosilicate material with three-dimensional network structure, which is prepared using precursor and alkali activator [23]. When used as a cementitious material, geopolymer exhibits excellent performance in early strength, durability, high-temperature resistance and acid resistance [24,25]. In contrast to

* Corresponding author.
* Corresponding author at: School of Civil Engineering and Architecture, Wuhan University of Technology, Luoshi Road 122, Wuhan 430070, China.
E-mail addresses: wusp@whut.edu.cn (S. Wu), xushi@whut.edu.cn (S. Xu).

https://doi.org/10.1016/j.conbuildmat.2024.139287
Received 25 June 2024; Received in revised form 13 October 2024; Accepted 18 November 2024
Available online 27 November 2024

cement, geopolymer can be produced without calcination, and a range of industrial solid waste can be chosen as precursors. Therefore, using geopolymer to prepare geopolymer foamed concrete (GFC) can reduce the dependence of traditional foamed concrete on cement, thereby reducing the large amount of CO_2 emissions produced by cement production [26,27].

So far, most researchers have selected silicon-aluminum solid waste materials as precursors for synthesizing GFC [28–31]. Hao et al. [32] prepared a high-strength GFC using fly ash (FA) and ground granulated blast furnace slag (GBFS) as precursors. They found that FA improved the volume stability of GFC paste, and GFC had better machinability and mechanical properties than cement-based foamed concrete. Badanoiu et al. [33] prepared GFC using red mud (RM) as precursors and characterized its high-temperature performance. The results showed that RM-based GFC had lower open porosity and higher compressive strength than cement-based foamed concrete at high temperature. However, there are relatively few studies about utilizing SS as precursor in the synthesis of GFC. Compared to traditional silicon-aluminum waste materials, the structure and properties of GFC prepared using SS as a precursor remain unclear and needs further in-depth research.

Furthermore, as a kind of lightweight high-strength material, the mechanical properties of GFC is crucial for its practical applications [34,35]. Previous research has demonstrated that the uniformity of pore distribution and skeleton strength are one of the primary factors affecting GFC's compressive strength [36–38]. To improve this, many studies have focused on using foam stabilizers to improve the pore diameter distribution of GFC to enhance its compressive strength [39]. Feng et al. [40] regulated the early strength of GFC using triethanolamine and found that triethanolamine increased the dissolution rate of precursors and improved the pore structure of GFC, thereby enhancing its early strength. Zhang et al. [41] found that using CO_2 as foam stabilizer can increase the paste's viscosity, leading to a more uniform pore distribution and finer pore diameter, thus enhancing foamed concrete's mechanical properties. Moreover, considering the practical application scenarios, there is a growing demand for GFC to possess excellent waterproofing and thermal insulation properties. Incorporating waterproofing and thermal insulation materials into GFC is the most feasible and widely adopted approach to achieve this goal. By adding polymethylhydrosiloxane (PMHS) to GFC, Dong et al. [42] prepared a kind of GFC with ultra-high hydrophobicity. They observed that PMHS formed hydrophobic alkylated nano-silicon fibers on the surface of GFC to achieve ultra-high hydrophobicity. Wang et al. [43] significantly reduced the thermal conductivity of GFC by adding hollow microspheres into GFC. The thermal conductivity decreased by 30.4 % when the percentage of hollow microspheres in GFC reached 50 %.

Emulsified asphalt (EA) is a kind of emulsion formed by mechanical shearing of asphalt and emulsifier, which has been widely used in cement-based materials [44–46]. EA has been proven to greatly improve cement-based materials' adhesion, durability, and crack resistance, thereby improving its overall performance and service life [47–49]. In addition, EA can also enhance the viscosity of cement paste and improve its uniformity [50,51]. Therefore, we believe that EA holds a significant potential to improve the pore structure of GFC and enhance its mechanical properties. Additionally, EA's excellent waterproofing and thermal insulation properties could contribute to improve the functional performance of engineering materials. Liu et al. [52] developed a semi-flexible composite mortar material with excellent waterproof properties using EA and magnesium sulfate cement. They found that after adding 10 % EA, the compressive strength of the mortar soaked in water for 28 days was basically the same as that before soaking, indicating that EA significantly enhanced the waterproof performance of the mortar. Razali et al. [53] utilized EA as an insulating coating to improve the thermal insulation properties of gypsum boards. The results demonstrated that the EA could significantly reduce the heat transfer of the gypsum board, and the higher the solid content of emulsified asphalt, the stronger the thermal insulation ability of the coating. However, the production of GFC with EA to improve its waterproofing and thermal insulation properties has not been investigated yet.

This study aims to develop a novel steel slag-based geopolymer foamed concrete (SSGFC) incorporating EA to stabilize its pore structure and improve its pore structure, compressive strength, water resistance and thermal insulation properties. Considering the poor dispersibility of EA in GFC paste, in this study, different contents of EA were directly mixed in the foaming solution, and the EA-modified foam was obtained by high-speed stirring and foaming. Then, the modified foam was uniformly mixed with steel slag-based geopolymer paste to prepare SSGFC. Firstly, the fresh properties of SSGFC paste were tested, including volume stability, fluidity, and setting time. Then, the reaction products, microstructure, and pore structure of SSGFC were investigated by X-ray diffraction (XRD), Fourier-transform infrared spectroscopy (FTIR), thermogravimetric analysis (TG-DTG), scanning electron microscopy (SEM) and X-ray computed tomography (X-CT). Finally, SSGFC's physical properties, including its compressive strength, water absorption and thermal conductivity, were evaluated. The findings of this study will offer theoretical support for the engineering application and performance improvement of SSGFC.

2. Materials and methods

2.1. Materials

SS, FA and GBFS were chosen as the precursors for the synthesis of geopolymer in this study. They were obtained from China Huaxin Cement Co., Ltd. X-ray fluorescence (XRF) test, XRD test and laser particle size test were performed on the precursors. The results are displayed in Table 1 and Fig. 1.

Table 1 showed that the main oxides of SS are CaO (45.38 %) and Fe_2O_3 (26.11 %), the main oxides of FA are SiO_2 (54.94 %) and Al_2O_3 (32.83 %), and the main oxides of GBFS are CaO (40.41 %) and SiO_2 (32.21 %). Fig. 1(a) indicated that the main crystalline phases in SS were C_2S, C_3S, C_3A, FeO and RO phases, while the three primary crystalline phases of FA were calcium oxide, quartz and mullite. The RO phase in SS refers to a solid solution of metal oxides, primarily consisting of FeO, CaO, and MgO, formed during the cooling and solidification of molten slag in steelmaking. Since GBFS underwent extremely rapid cooling during its generation, the majority of its composition was glass phase, as evidenced by the distribution of bumps from $2\theta=20^\circ$ to $2\theta=40^\circ$ in its XRD patterns. Fig. 1(b) illustrated that the average particle sizes of SS, FA and GBFS were relatively small, which were 48.31μm, 11.37μm and 32.62μm, respectively. The smaller particle size is beneficial to increase the region of interaction between precursors and alkaline activator, thereby increasing the reaction rate of geopolymerisation [54,55].

Using water glass as the alkaline activator for precursors, Table 2 presents its fundamental characteristics. Before preparing SSGFC, the water glass's modulus was adjusted to 1.5 using sodium hydroxide (NaOH), and then the water glass was allowed to stand for 24 h to maintain the stability of the modulus.

The EA used in this study is a kind of cationic EA with the solid content of 55 %. It was purchased from a building materials company in Taizhou City, China. Its basic properties are shown in Table 3.

In this study, sodium dodecyl sulfate (SDS) and hydroxypropyl methylcellulose (HPMC) were utilized as the foaming agent and foam stabilizer, respectively. SDS is an anionic surfactant with excellent foaming ability and chemical stability in alkaline environments, making it suitable for alkaline geopolymer pastes. HPMC is a water-soluble polymer known for its excellent film-forming and water-retaining properties, so it is often used as foam stabilizer in foamed concrete [56]. SDS and HPMC were added in water at the weight ratio of 1:0.1:25 and stirred at 200 rpm for 2 h at 25 °C to prepare foaming solution.

Table 1
The chemical compositions of SS, FA and GBFS.

Raw materials	Oxide type	SiO_2	Al_2O_3	CaO	Fe_2O_3	MgO	Na_2O	K_2O	P_2O_5	MnO	LOI
SS	Oxide content (%)	11.81	1.93	45.38	26.11	3.82	0.16	0.11	1.93	2.92	3.82
FA		54.94	32.83	2.42	3.01	0.94	0.72	1.74	0.21	0.04	1.47
GBFS		32.21	15.03	40.41	0.51	7.42	0.37	0.45	0.02	0.15	1.18

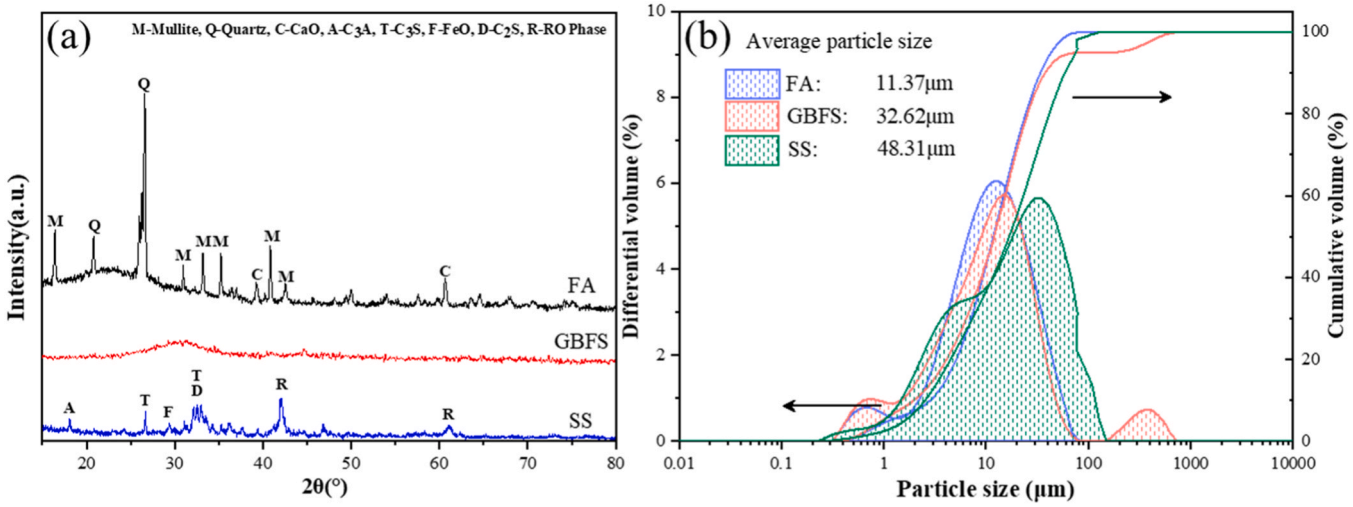

Fig. 1. XRD patterns and particle size distribution of SS, FA and GBFS, (a) XRD patterns, (b) particle size distribution.

Table 2
Essential characteristics of water glass.

Properties	Value
Solid content / %	34.91
SiO_2 content / %	25.86
Na_2O content / %	8.15
Baume degrees	39.80
Modulus	3.29

Table 3
Basic properties of EA.

Properties	Value
Solid content / (%)	55.20
Density / (g/cm^3)	1.01
Surface dry time / (h)	4.10
Fracture elongation / (%)	632.20
Tear strength / (N/mm)	62.10

Table 4
The mixing proportions of raw materials.

Groups	Composition of precursors			EA content/ % by total weight of foaming solution	Foam/ g	Water/ g	Water glass/g
	SS/ g	FA/ g	GBFS/ g				
FC-EA0	200	120	80	0	15	98	174
FC-EA5	200	120	80	5	15	98	174
FC-EA10	200	120	80	10	15	98	174
FC-EA15	200	120	80	15	15	98	174
FC-EA20	200	120	80	20	15	98	174

Note: In this study, the total weight of the foaming solution used to prepare each group of modified foam was 100 g.

2.2. Mix proportions and preparation of samples

The preparation of SSGFC samples mainly involves four steps: i) preparation of foaming solution, ii) preparation of foam, iii) preparation of SSGFC paste and iv) casting and curing. Table 4 displays the mix proportions of SSGFC samples. Before foaming, 5 %, 10 %, 15 % and 20 % (by weight of foaming solution) of EA were added to the foaming solution prepared from SDS and HPMC respectively and stirred at 200 rpm for 10 minutes. Then, the foaming solution was stirred at 2000 rpm for 1 minute to obtain modified foam. The precursor, water glass and water were uniformly mixed according to the proportions in Table 4 to prepare geopolymer paste. The water-to-binder ratio used in this study was fixed at 0.5. In calculating the amount of water to be added, the total weight of water is first determined based on the total weight of the precursor and the water-to-cement ratio. Next, the weight of water contained in water glass is calculated according to its solid content and weight. The difference between these two values represents the weight of the water that needs to be added. Since the foam plays a role in filling the SSGFC slurry and does not participate in the hydration reaction, the weight of water in the foam is negligible. The following equation is used to calculate the amount of water glass depending on the Na_2O dosage (D_{Na2O}):

$$m_1 = \frac{D_{Na_2O} \cdot m_P}{P_{Na_2O}} \quad (1)$$

Where m_P is the weight of the precursors (g), D_{Na2O} is the percentage of Na_2O weight in water glass to the weight of the precursor (%), P_{Na2O} is the content of Na_2O in the water glass (wt%) and m_1 is the amount of water glass (g).

The geopolymer paste was mixed with modified foam for 90 s at 94 rpm in the mixer to produced fresh SSGFC paste. The fresh paste was quickly poured into a mold with the size of 40 mm×40 mm×40 mm, covered with plastic film and placed in the oven at 60 °C for 24 h. The

SSGFC samples were then demolded and further cured in the curing chamber (20±2°C, 95±2 % RH) for an additional 2d and 27d before testing. The entire preparation process of SSGFC samples is shown in Fig. 2.

2.3. Testing methods

2.3.1. Measurement of fresh properties

2.3.1.1. Paste settlement. The decomposition of foam in fresh SSGFC paste will lead to settlement, so the stability of foam in SSGFC paste can be measured by measuring the settlement value of fresh paste in a certain period of time [41]. A certain amount of fresh paste was put into a 250 ml measuring cylinder, and the initial height was recorded as h_0. After standing for 10 min, 20 min and 30 min, the height of the paste was recorded as h_t, and the settlement value of the paste can be calculated by the following equation [56]:

$$SV = \frac{h_0 - h_t}{h_0} \times 100\% \quad (2)$$

Where SV is the settlement value of SSGFC paste (%), h_0 is the initial height of fresh paste (mm), and h_t is the height of the paste at time t (mm).

2.3.1.2. Fluidity. The fresh SSGFC paste's fluidity was measured using a hollow cylinder with an inner diameter and height of 80 mm according to the Chinese standard CJJ/T 177–2012. [57] The hollow cylinder was placed on a smooth glass plate, and after filling the cylinder with fresh paste, the top surface of the cylinder was scraped flat, and the cylinder was lifted vertically within 3 s. After the paste flowed freely for 1 min, the fluidity value was determined by measuring the paste's flow diameter. Three measurements were made for each group of SSGFC paste, and the average value with standard deviation was reported.

2.3.1.3. Setting time. Different from the high-viscosity cement paste, the addition of foam results in a lower viscosity, higher fluidity, and reduced early strength of the SSGFC paste. Consequently, the setting time of the SSGFC paste could not be accurately measured using a Vicat apparatus. Therefore, in this study, the setting time of fresh SSGFC paste was determined based on references. [41,58,59]. Firstly, the precursor was mixed with water and water glass to prepare geopolymer paste, and the time at this point was recorded as T_0. Then the geopolymer paste was mixed with modified foam to prepare fresh SSGFC paste. 200 g of the paste was poured into a 500 ml beaker, and within 10 s, the beaker was slowly tilted to the horizontal position. This operation was repeated until the paste surface did not flow when the beaker was tilted to the horizontal position. This moment was considered as the solidification state of the paste, and the time was recorded as T_1. The setting time of the paste is the difference between T_1 and T_0. After three measurements were made for each group of SSGFC paste, the average value with standard deviation was reported.

The testing process for the paste settlement, fluidity and setting time of fresh SSGFC paste is shown in Fig. 3.

2.3.2. Microscopic analysis

The central part of SSGFC samples after 7d of curing were broken and immersed in anhydrous ethanol for 7d to stop hydration, and then dried at 40 °C for 24 h. In preparation for XRD, TG-DTG, and FTIR tests, the dried sample was ground into powder with a particle size of less than 0.075 mm. The thermogravimetric analyzer (Henven HTG-1, China) was set to heat at a rate of 10 °C per minute. Additionally, the temperature rose to 1000 °C from 0 °C. The infrared spectrometer (Delite DH108, China) was configured with a detection wavenumber of 400–4000 cm^{-1}. SEM (Zeiss Gemini 300, Germany) testing was performed on the dried block samples to examine the microstructure, pore morphology, and reaction products of SSGFC. To enhance the imaging quality, a platinum layer was plated on the sample's surface before testing.

2.3.3. X-ray computed tomography (X-CT)

The pore size distribution inside SSGFC sample was investigated by X-CT (Zeiss Xradia 510 Versa, GER). To reduce the impact of the irregular surface, a region with dimensions of 20×20×20 mm^3 in the sample's center was chosen for testing. The sample was scanned under a beam current of 120 μA and an acceleration voltage of 120 kV. The original data collected by the high-resolution detector were imported into Dragonfly 4.1 software for pore parameter analysis, including

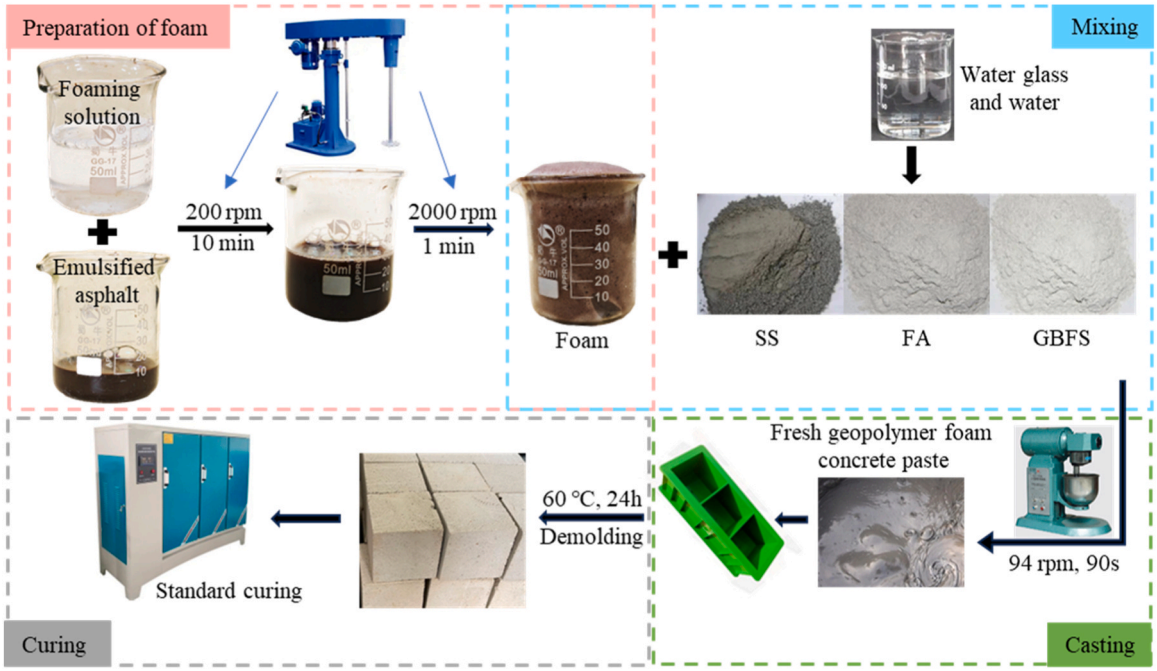

Fig. 2. The entire preparation process of SSGFC samples.

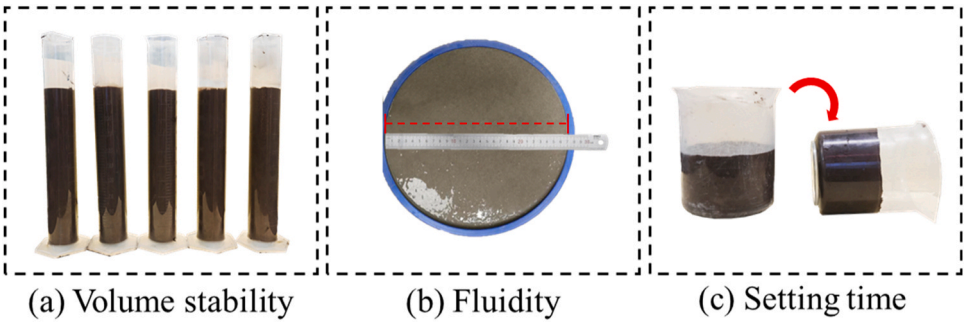

Fig. 3. Measurement of fresh properties, (a) volume stability, (b) fluidity, (c) setting time.

porosity, pore diameter distribution and non-connected pore volume ratio. Three measurements were made for each group of SSGFC samples to ensure the accuracy of the conclusions. According to the previous study [60], the pore diameter distribution of foamed concrete conforms to the normal distribution. Therefore, to explore the pore diameter distribution of SSGFC samples, the pore diameter distribution is fitted according to the following functions[61]:

$$f(D) = \frac{1}{\sigma\sqrt{2\pi}}\exp^{(-\frac{(D-\mu)}{2\sigma^2})} \quad (3)$$

Where D is the pores diameter, μ and σ are the mean and standard deviation of the pores diameter.

2.3.4. Measurement of physical properties

2.3.4.1. Compressive strength. According to the Chinese standard JG/T 266–2011 [62], the compressive strength of SSGFC samples at 3d and 28d was measured. Each group of samples was tested six times, and the average value with standard deviation was reported. Additionally, to minimize the influence of differences in dry density on compressive strength, based on the dry density and compressive strength of the samples, the specific strength of the samples was calculated using the following equation [40]:

$$S = \frac{S_0}{D} * 10^6 \quad (4)$$

Where S is the specific strength of SSGFC samples (N·m/kg), S_0 is the compressive strength of SSGFC samples (MPa), D is the dry density of SSGFC samples (kg/m^3).

2.3.4.2. Water absorption. According to the Chinese standard JG/T 266–2011 [62], the water absorption of SSGFC was measured. Firstly, the 28d cured SSGFC samples were dried to constant weight in an oven at 60°C. Then, they were placed in a constant temperature water bath at 20±5°C, with the liquid level reaching one-third of the sample height, and kept insulated for 24 h. Subsequently, water was added until the liquid level reached two-thirds of the sample height, and the insulation was continued for another 24 h. Finally, water was added until the liquid level exceeded the sample height by more than 30 mm, and insulation was maintained for 24 h. The SSGFC samples' water absorption was calculated by the following equation:

$$W_R = \frac{m_g - m_0}{m_0} \times 100\% \quad (5)$$

Where W_R is water absorption, m_0 is the weight of SSGFC samples after drying, m_g is the weight of SSGFC samples after water absorption. Three measurements were made for each group of SSGFC paste, and the average value with standard deviation was reported.

2.3.4.3. Thermal conductivity. The SSGFC samples cured for 28d were dried to constant weight in an oven at a temperature of 60 °C, and then the thermal conductivity of SSGFC samples at room temperature was tested using Hot Disk Thermal Analyzer (as shown in Fig. 4(a)). For each group of samples, the probe is clamped in the central area of the two samples to form a sandwich-like structure (as shown in Fig. 4(b)), and then the compression screw is adjusted to reduce the gap between the probe and the sample. The sample's thermal conductivity was tested using the transient flat heat source method. The test time is set to 120 s, and the test power is 60 mW. Three measurements were made for each group of SSGFC paste to ensure the accuracy of the results.

3. Results and discussion

3.1. Properties of fresh paste

3.1.1. Paste settlement

Fig. 5 illustrates the settlement values of different groups of fresh SSGFC pastes over time, while Fig. 6 shows the foam and modified foam observed by digital microscope. From Fig. 5, it can be observed that the settlement value of fresh paste increased with time. Compared to the control group FC-EA0, when the EA content in the modified foam was increased from 0 % to 5 % and 10 %, the settlement values of pastes at 30 minutes decreased from 2.7 % to 1.9 % and 1.5 %, respectively, indicating that EA enhanced the volume stability of the fresh SSGFC pastes. As shown in Fig. 6, EA can form a layer of film in the paste to increase its viscosity. This film can wrap the foam, preventing them from moving or separating in the paste, thereby enhancing the stability of the paste. However, when the EA content in the modified foam exceeded 10 %, the settlement values of the paste increased. This is because in the alkaline geopolymer paste, Ca^{2+} and Al^{3+} dissolved from SS, FA, and GBFS particles will make the surface of the precursor particles positively charged, while cationic EA will also make the foam's surface positively charged. Therefore, when the EA content exceeds the critical value (10 %), the electrostatic repulsion force of the precursor particles on the foam will be greater than the friction force of the foam in the paste, resulting in the movement and separation of the foam, thus reducing the volume stability of the paste.

3.1.2. Fluidity and setting time

The results of fluidity and setting time of different groups of fresh SSGFC pastes are displayed in Fig. 7. From Fig. 7(a), it is evident that the fluidity decreased with the increase of EA. In comparison to the control group FC-EA0, when the EA content in the modified foam increased to 20 %, the fluidity of SSGFC paste decreased from 288 mm to 269 mm, which can be attributed to three factors: firstly, the EA film will wrap the foam and precursor particles, thus increasing the viscosity of the paste. Secondly, the EA film will make the surface of the precursor particles hydrophobic. In the SSGFC paste, the hydrophobic precursor particles will aggregate and agglomerate, thereby reducing the fluidity of the paste, which is consistent with the conclusion of Zhang et al. [41]. Additionally, as mentioned in Section 3.1.1, When the EA content in the

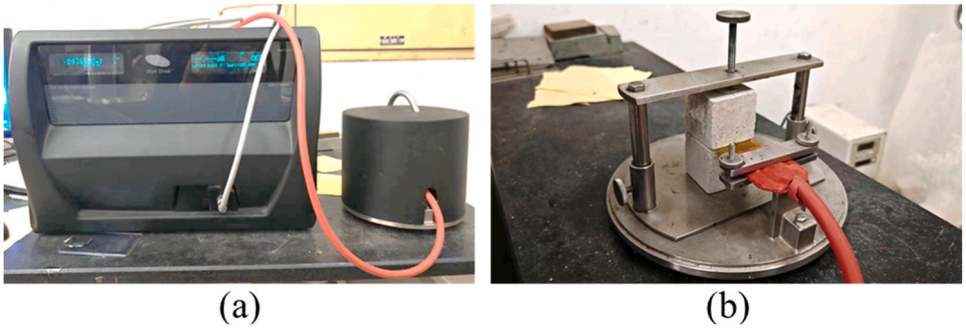

Fig. 4. Thermal conductivity test. (a) Hot Disk device; (b) Placement of samples.

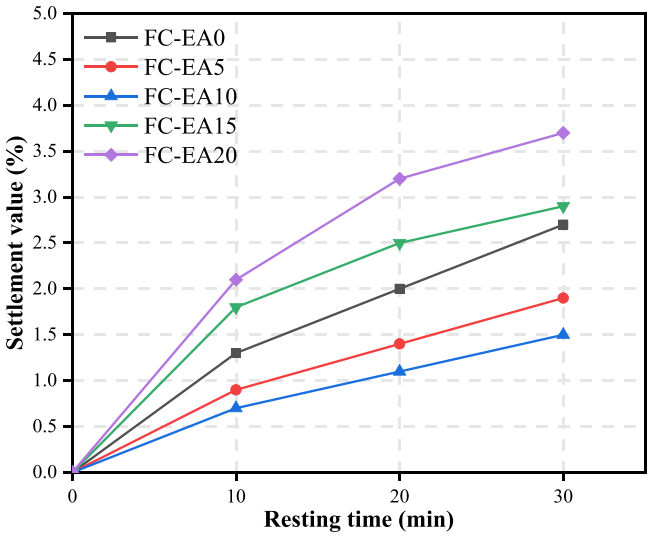

Fig. 5. Settlement values of different groups of fresh SSGFC pastes.

modified foam exceeds 10 %, the foam content in the paste will decrease, thereby increasing the friction between the particles and lead to the decrease of fluidity [63].

In terms of setting time, as shown in Fig. 7(b), the setting time of SSGFC fresh paste increased slightly with the increase of EA content. Compared with the control group FC-EA0, when the EA content in the modified foam increased to 20 %, the setting time of the paste increased from 37 min to 45 min. This may be because the EA film covered the surface of the precursor particles, hindering the contact of the precursor particles with water glass, thereby reducing the rates of hydration and geopolymerisation reactions. In addition, alkaline conditions facilitate the catalysis of geopolymerization reaction [64]. However, the cations in EA will react with anions such as OH^- in water glass, thereby reducing the alkalinity of the cementitious system and slowing down the rate of geopolymerization reaction.

3.2. Microscopic analysis

3.2.1. Reaction products analysis

Fig. 8 display the XRD and FTIR results of different groups of SSGFC samples. From Fig. 8(a), it can be observed that after curing for 28d, the main mineral phases present in the samples are mullite (Al_2O_3), quartz (SiO_2), calcium aluminosilicate hydrate (C-A-S-H) and calcium silicate hydrate (C-S-H). Combined the oxide compositions of the three precursors, it can be judged that the mullite phase mainly originates from unreacted FA in SSGFC samples, while the quartz phase comes from both FA and GBFS. As two kinds of solid wastes with high calcium content, when used as geopolymer precursors, SS and GBFS will accelerate the development of C-S-H gel and C-A-S-H gel under alkaline conditions [23]. As the primary reaction products, the structure of C-S-H gel and C-A-S-H gel in SSGFC is similar to zeolite. They are amorphous phase materials, so they cannot produce strong Bragg reflection like crystal structure, appearing as continuous peaks at 2θ=28–35° in Fig. 8(a). The FTIR results of different groups of SSGFC samples are shown in Fig. 8(b), it is evident that the infrared spectra of each group of samples are basically the same. The two vibration bands at 3446 cm^{-1} and 1647 cm^{-1} belong to the stretching and bending vibrations of O-H bonds in bound water of hydration products. The vibration band at 974 cm^{-1} is attributed to the asymmetric stretching vibration of Si-O-Si (Al) bonds, while the two bands at 452 cm^{-1} and 678 cm^{-1} are attributed to the bending vibrations of Si-O-Si bonds. These three vibration bands prove the existence of C-(A)-S-H gel. The vibration band at 721 cm^{-1} is attributed to the vibration of Al-O. Weak vibration bands at 1422 cm^{-1} and 1475 cm^{-1} belong to the bending vibrations of C-O bonds, indicating the presence of slight carbonation in SSGFC samples. The sample's infrared spectra remained unchanged after the addition of EA, which agreed with the results of XRD. It can be concluded that the reaction product of SSGFC will not change with the addition of EA, and the

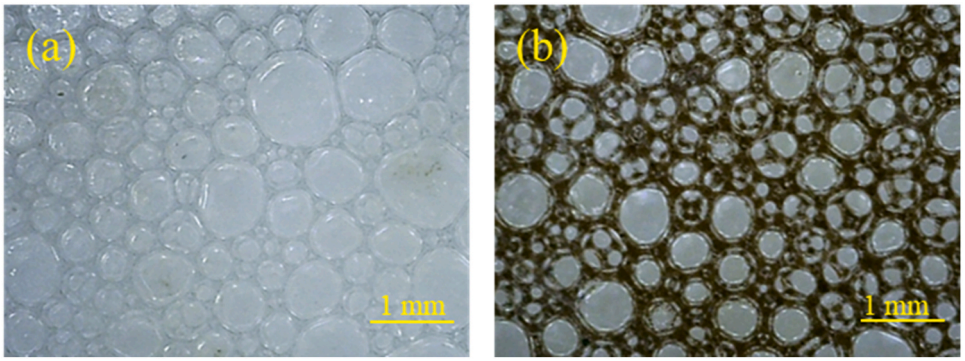

Fig. 6. The morphology of foam and modified foam, (a) foam, (b) modified foam.

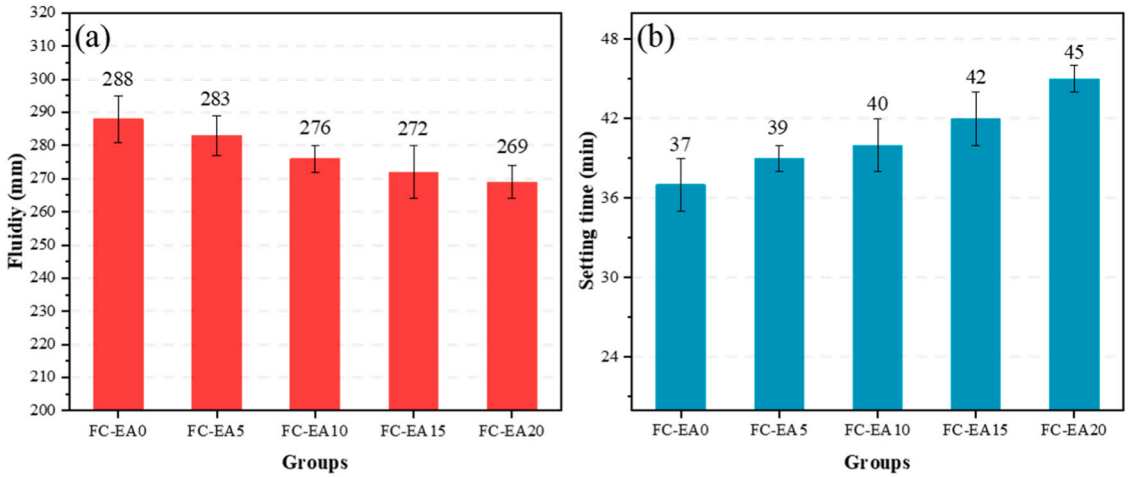

Fig. 7. Fluidity and setting time of each group of fresh SSGFC pastes, (a) Fluidity, (b)Setting time.

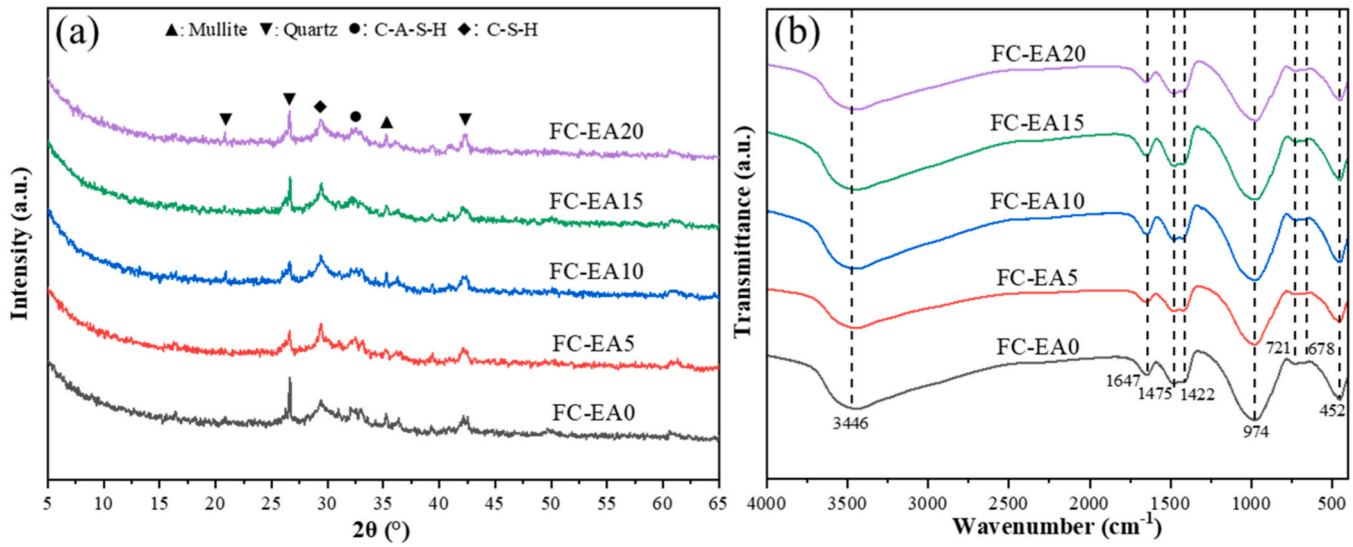

Fig. 8. XRD and FTIR results of different groups of SSGFC samples, (a) XRD, (b) FTIR.

primary product is C-(A)-S-H gel.

3.2.2. TG-DTG analysis

Fig. 9 presents the TG-DTG curves of different groups of SSGFC samples after curing for 28d. The SSGFC samples exhibit significant weight loss in the two temperature ranges of 20–200 °C and 700–800 °C. Based on previous studies [23], the weight loss of geopolymer between 20 and 200 °C is linked to the thermal breakdown of C-A-S-H gel, while the weight loss in 700–800°C is associated with the thermal breakdown of $CaCO_3$. This indicated that C-(A)-S-H gel was the sample's primary hydration product, and the sample was carbonated, which agrees with results of XRD test.

By quantitatively analyzing the weight loss of the sample in the temperature range of 20–200 °C, the amount of hydration products of different groups of SSGFC samples can be compared. As shown in Fig. 9, when the EA content in modified foam increased from 0 % to 5 %, 10 %, 15 %, and 20 % respectively, the weight loss of the samples in 20–200 °C decreased from 11.66 % to 11.23 %, 11 %, 10.71 %, and 10.66 % respectively, indicating that EA has an adverse impact on the hydration of SSGFC. This may be attributed to several factors. Firstly, the EA film hinders the contact between precursor particles and water glass. Secondly, the cations in EA react with anions such as OH^-, reducing the alkalinity of the system and thus lowering the rate of hydration reaction. Additionally, as shown in the reaction Eqs. (6–8), the reaction monomers such as $[H_3SiO_4]^-$, $[H_3AlO_4]^{2-}$, and $[Al(OH)_6]^{3-}$ produced by the silico-aluminous components in the precursors under alkaline conditions will be attracted by cations through electrostatic forces [65], thereby hindering the progress of geopolymerization reactions and resulting in a decrease in reaction products.

$$SiO_2 + OH^- + H_2O \rightarrow [H_3SiO_4]^- \quad (6)$$

$$AlO_2^- + OH^- + H_2O \rightarrow [H_3AlO_4]^{2-} \quad (7)$$

$$AlO_2^- + OH^- + H_2O \rightarrow [AlOH_6]^{3-} \quad (8)$$

3.2.3. SEM

Fig. 10 depicts the SEM images of different SSGFC samples after curing for 28d. From Fig. 10(a), (c), and (e), it is evident that when the EA content in the modified foam increased to 10 %, compared with the control group FC-EA0, FC-EA10 exhibited a greater number of pores with more uniform pore diameter. However, when the EA content in the modified foam increased to 20 %, the number of pores in FC-EA20 significantly decreased, and the density of the sample increased. This is because as described in Section 3.1.2, the EA film not only enhances the stability of the foam but also increases the viscosity of the paste,

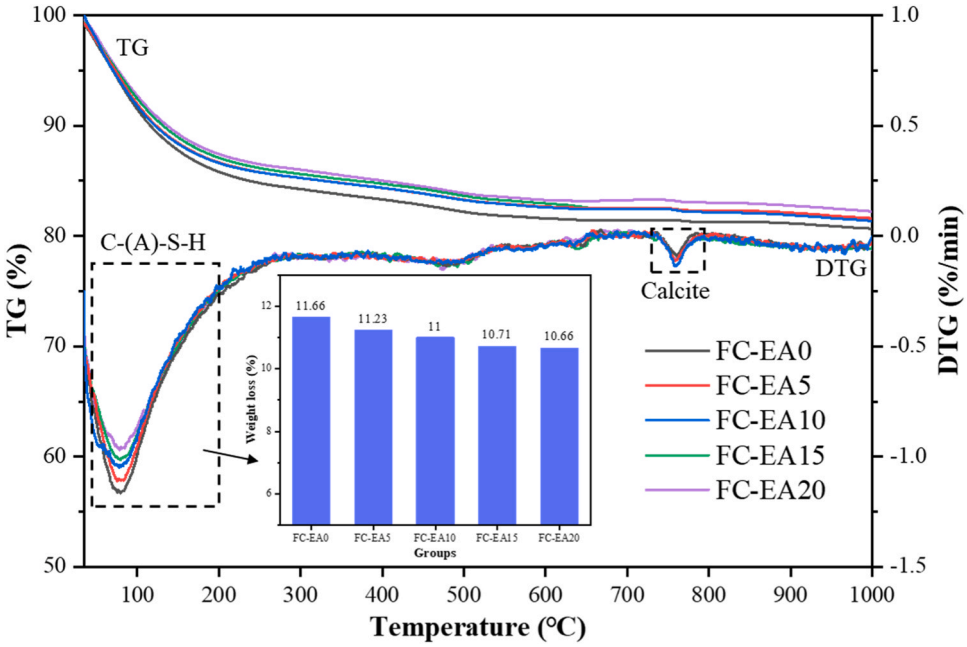

Fig. 9. TG-DTG curves of different groups of SSGFC samples.

hindering the foam's movement in the paste. Therefore, the addition of EA can improve the pore structure of SSGFC. However, when excessive EA was added, the foam in the paste became unstable due to electrostatic forces, resulting in movement and separation of the foam, leading to a decrease of pores and consequently reducing the porosity of the SSGFC sample. Fig. 10(b) and (f) respectively show the pore morphology of FC-EA0 and FC-EA20. It can be observed that the inner surface of the pores in FC-EA20 is smoother, while the inner surface of pores in FC-EA0 is covered with reaction products generated by hydration and geo-polymerization reactions, indicating that FC-EA0 had a higher degree of hydration, which agrees with the results of TG-DTG test. From Fig. 10 (d), the C-(A)-S-H matrix gel produced inside the SSGFC sample can be observed. A large number of matrix gels form a gel network inside the sample, which provides support for the strength of SSGFC.

3.2.4. X-CT

Fig. 11 shows the pore diameter distribution and the three-dimensional pore structure of SSGFC samples based on X-CT. Table 5 lists the average pore diameter, porosity, non-connected pore volume ratio and pore diameter normal distribution fitting results of SSGFC samples. From Fig. 11(a), It is evident that as EA content increased, the peak of the curve gradually moved to the direction of smaller pore diameter, indicating that the average pore diameter of the sample decreased. As the EA content rose from 0 % to 10 %, the average pore size of the sample decreased from 418 μm to 411 μm, while the porosity increased from 23.27 % to 24.4 %. Additionally, the value of σ decreased from 99.8 to 87.2. According to the study of Li et al. [66], a smaller σ implies a more concentrated pore distribution. This implies that the addition of EA helps to improve the pore diameter distribution of SSGFC. This may be because the EA film not only enhanced the foam's stability in the paste, but also enhanced the paste's viscosity and inhibited the coalescence of the foam, thereby reducing the average pore diameter of SSGFC and optimizing its pore size distribution.

According to the conclusion in Section 3.1.1, when the EA content exceeded 10 %, the foam's stability in the paste began to decrease due to the effect of electrostatic force. However, in Table 5, when the EA content increased from 10 % to 15 % and 20 %, the average pore diameter and the value of σ still maintained a downward trend, and the porosity also decreased from 24.4 % to 20.96 % and 20.14 %, respectively. This may be because that with the increase of EA content, the large foam in the paste was separated and broken under stronger electrostatic force, leading to a decrease in the porosity and an overall reduction in pore diameter. It is noteworthy that the non-connected pore volume ratio of SSGFC samples in Table 5 shows the same variation trend to the porosity. When the EA content increases from 0 % to 10 %, the volume ratio of non-connected pores increases from 9.89 % to 11.16 %, accounting for 45.7 % of the total pore volume. Although when the EA content further increases to 20 %, the volume ratio of non-connected pores decreases to 10.33 %, at this point, the volume of ratio of non-connected pores in samples accounts for 51.3 % of the total pore volume, demonstrating that the addition of EA will hinder the foam's movement in the paste, thereby reducing the probability of foam merging to form connected pores.

3.3. Physical properties

3.3.1. Compressive strength

Fig. 12 shows the dry density, compressive strength and specific strength of different groups of SSGFC samples after curing for 3d and 28d. It is evident that when the amount of EA in the sample increases, the dry density of the sample shows a trend of decreasing first and then increasing, which is contrary to the results of the porosity. This is because the dry density of foamed concrete is inversely proportional to the porosity, and lower porosity means a denser skeleton structure and higher strength [66]. However, it is evident in Fig. 12 that even when the dry density of the samples decreased, the 28d compressive strength of FC-EA10 (9.1 MPa) increased by 21.4 % compared to FC-EA0 (7.5 MPa), and the 28d specific strength of FC-EA10 (9137 N·m/kg) increased by 25.4 % compared to FC-EA0 (7289 N·m/kg). This indicates that FC-EA10 has higher strength than FC-EA0 at the same weight. This is because, as described in Section 3.2.4, the addition of EA improves the pore diameter distribution of SSGFC and reduces the average pore diameter, which means that more small pores are evenly distributed throughout the SSGFC samples. Such a pore structure can make the stress more evenly distributed in the concrete, reduce the possible local stress concentration, and thus improve the overall strength. As the EA content increased from 10 % to 15 % and 20 %, the SSGFC samples' compressive strength significantly increased due to the reduction in porosity. The 28d compressive strength of FC-EA15 and FC-EA20 (10.5 MPa and 11.2 MPa) increased by 40 % and 49 % compared to

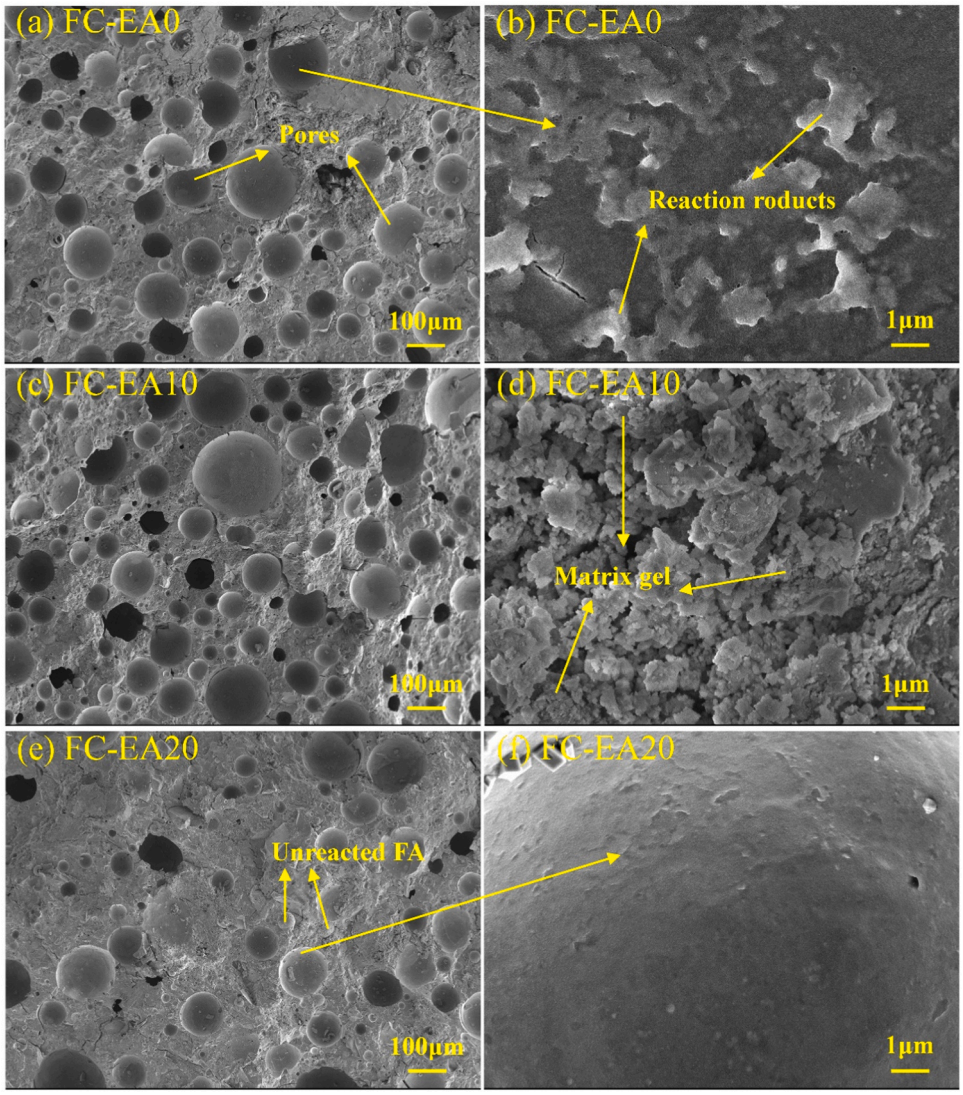

Fig. 10. SEM images of geopolymer foamed concrete, (a) FC (×100), (b) FC (×10000), (c) FC-EA10 (×100), (d) FC-EA10 (×10000), (e) FC-EA20 (×100), (f) FC-EA20 (×10000).

FC-EA0. However, the specific strength of FC-EA20 (9764 N·m/kg) showed only little change compared to FC-EA15 (9686 N·m/kg). This is because, as shown in Table 5, there was not a noticeable difference in pore parameters between FC-20 and FC-EA15.

3.3.2. *Water absorption*

Fig. 13 presents the water absorption results of different groups of SSGFC samples. It is evident that when the EA content increased, SSGFC's water absorption decreased. The water absorption of FC-EA0 was 39.6 %. When the EA content increased to 20 %, the water absorption of FC-EA20 decreased to 29.6 %, which was 25.3 % lower than FC-EA0. This is because the lower porosity of FC-EA20 will lead to a decrease in its water absorption. However, FC-EA5 and FC-EA10 still exhibit lower water absorption (35.1 % and 33.1 %, respectively) than FC-EA0 despite having a higher porosity than FC-EA0. Therefore, it can be concluded that the addition of EA significantly reduces the water absorption of SSGFC. This may be attributed to three factors. Firstly, the EA film can form a covering layer at the pores, which hinders the water directly into the pores of SSGFC and slows down the rate of water penetration, thereby reducing the water absorption. Secondly, EA is a kind of material with good hydrophobicity. Therefore, the addition of EA in SSGFC can increase the hydrophobicity of pores, thus effectively reducing the penetration of water into SSGFC and reducing the water absorption, which agrees with the conclusions of Qu et al. [67]. Additionally, the surfactants in EA can reduce the surface energy of SSGFC, thereby increasing the surface tension of SSGFC, which helps to reduce the absorption and penetration of water on the surface of SSGFC [68].

3.3.3. *Thermal conductivity*

Thermal conductivity is one of the most important performance indexes of foamed concrete. Smaller thermal conductivity means better thermal insulation capability. Previous studies have shown that the thermal conductivity of foamed concrete will decrease with the increase of porosity [69]. Fig. 14 shows the thermal conductivity of different groups of SSGFC samples. It is evident that the thermal conductivity of the samples exhibits a trend of initially decreasing and then increasing as the EA content increases. When the EA content increased to 10 %, the thermal conductivity of FC-EA10 was 0.255 W/mk, which was 31.3 % lower than FC-EA0 (0.371 W/mk). Even though the decrease in porosity led to an increase in the thermal conductivity of FC-EA15 and FC-EA20 (0.341 W/mk and 0.344 W/mk, respectively), they still remained lower than FC-EA0, which demonstrates that EA will significantly enhance the thermal insulation capability of SSGFC.

As shown in Fig. 15(a), the single foam in the SSGFC paste was influenced by various forces, including the frictional force (Ff), bubble confinement force (Fc), bubble buoyancy force (Fb), drainage force (Fd),

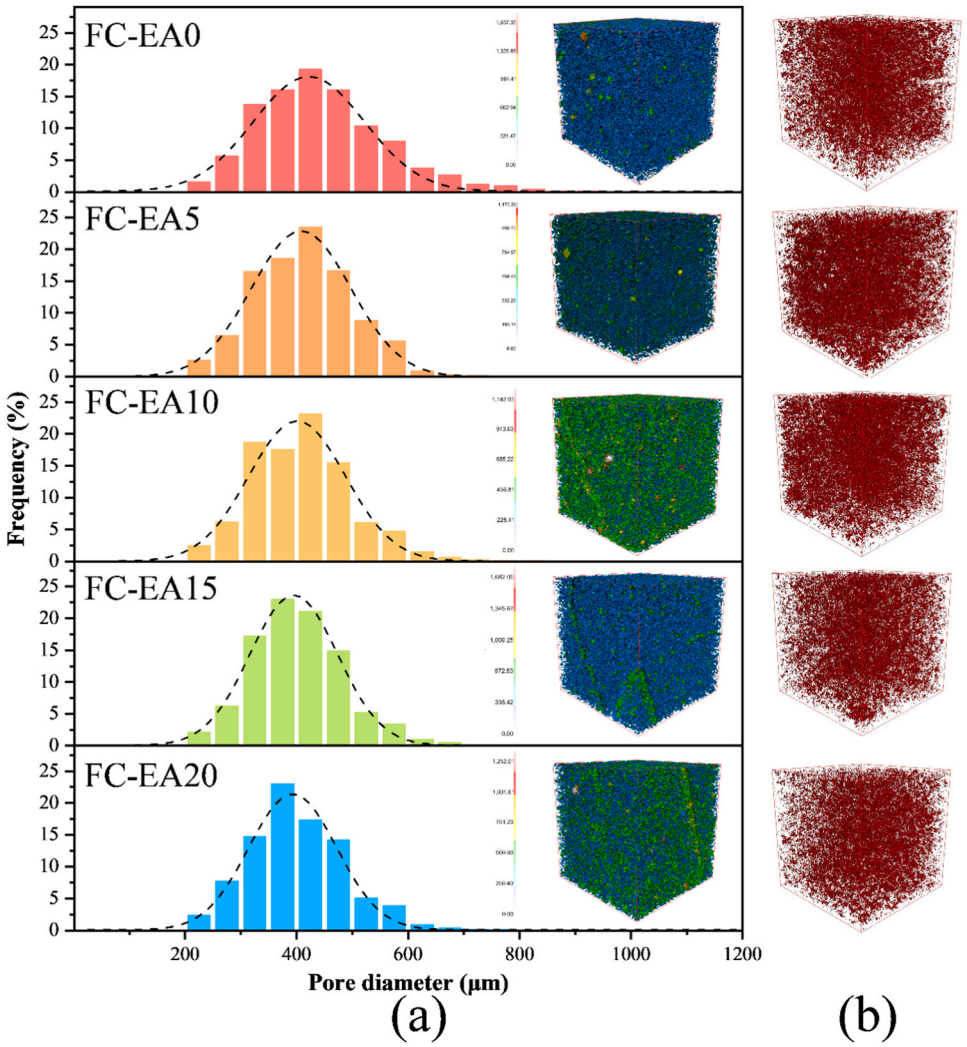

Fig. 11. X-CT results of SSGFC samples, (a) Pore diameter distribution and the three-dimensional pore structure, (b) the three-dimensional non-connected pore structure.

Table 5
Pore parameters of SSGFC samples.

Group	Average diameter (μm)	Porosity (%)	Non-connected pore volume ratio (%)	Standard deviation (σ)	Mean value (μ)
FC-EA0	418	23.27	9.89	99.8	422
FC-EA5	416	23.42	10.24	89.5	408
FC-EA10	411	24.4	11.16	87.2	400
FC-EA15	398	21.36	10.62	78.5	394
FC-EA20	392	20.14	10.33	78.4	392

surface tension (Fst) and internal bubble pressure (Fpb) [70]. The frictional coefficient between SSGFC paste and foam determines the magnitude of Ff, with the roughness of paste being the primary factor affecting this coefficient. From the results of Section 3.1.2, it is evident that the addition of EA reduces the fluidity of SSGFC paste, indicating that EA increases the friction between foam and paste. As depicted in Fig. 15 (b), the increase of Ff and the encapsulation of foam by EA will hinder the foam's motion within the paste, thereby reducing the coalescence and disproportionation of foam, resulting in a more uniform pore structure. From the perspective of pore structure, in the case of uneven pore size distribution, a shorter heat conduction path will be formed between the large pores, because heat can be transmitted directly through these large pores, resulting in an increase in thermal conductivity. Conversely, a more uniform pore size distribution reduces these direct heat transfer pathways, resulting in an overall reduction in thermal conductivity. From the perspective of material characteristics, EA has excellent thermal insulation performance, which can hinder the transmission of heat. Therefore, EA can form a thermal insulation layer in SSGFC structure, reducing the heat transfer of SSGFC samples, thereby reducing the thermal conductivity of SSGFC. In addition, EA can also change the conduction path of heat in SSGFC and increase the resistance of heat conduction, thereby slowing down the transmission speed of heat in SSGFC and leading to a decrease in thermal conductivity.

4. Conclusions

This study aimed to use EA modified foam to enhance the pore structure and physical properties of SSGFC. The effects of EA on the reaction products, microstructure, compressive strength, water absorption and thermal insulation performance of SSGFC were investigated. The main conclusions drawn from the experimental results are as follows:

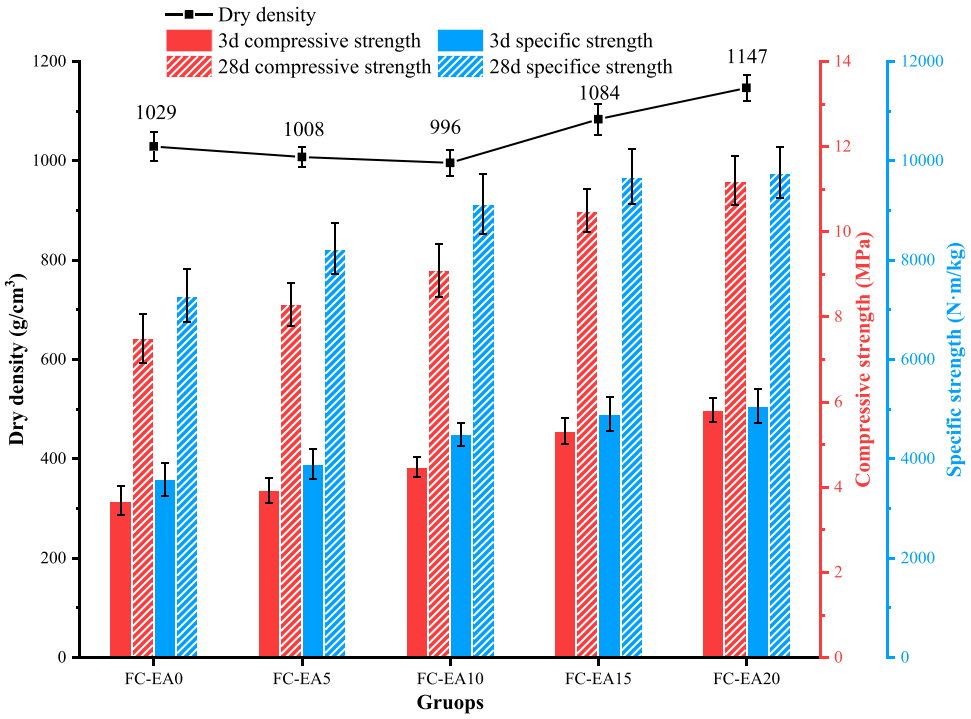

Fig. 12. Dry density, compressive strength and specific strength of different groups of SSGFC samples.

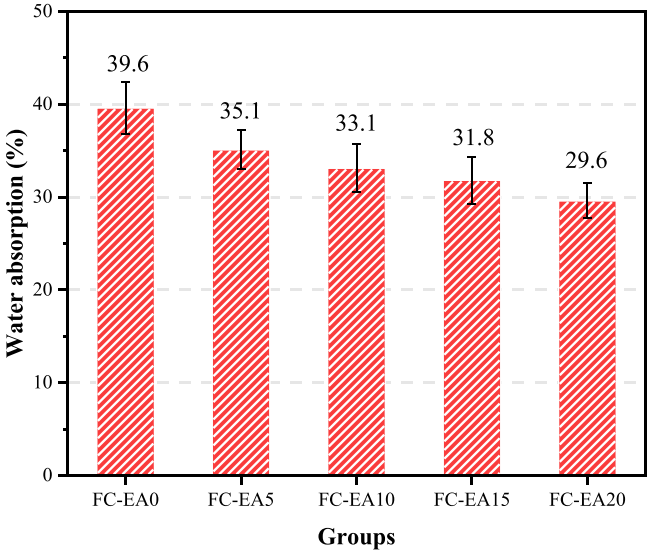

Fig. 13. Water absorption results of different groups of SSGFC samples.

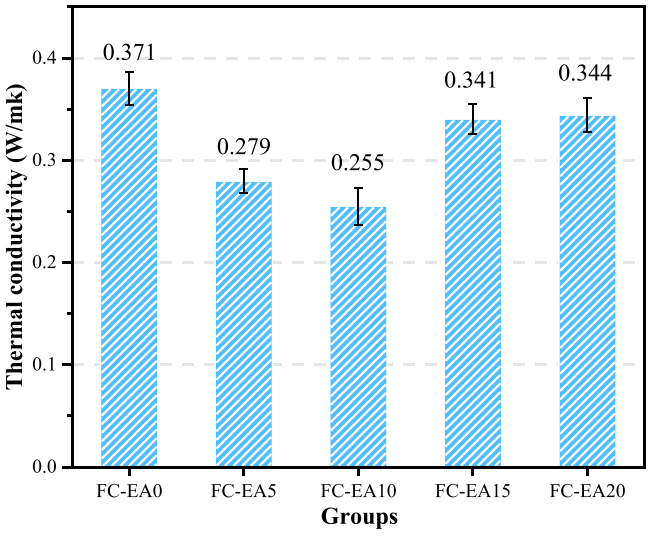

Fig. 14. Thermal conductivity of different groups of SSGFC samples.

(1) The addition of EA reduces the fluidity of fresh SSGFC paste, increases the setting time of fresh SSGFC paste, and improves the volume stability of fresh SSGFC paste. However, when the EA content in the modified foam exceeds 10 %, the electrostatic force between the foam and the precursor particles will reduce the volume stability of the SSGFC paste.

(2) The results of XRD, FTIR and TG-DTG showed that the reaction products of SSGFC did not change with the addition of EA, and the main product was C-(A)-S-H gel. However, the addition of EA reduced the alkalinity of the paste and hindered the contact between precursor particles and water glass, which will reduce the rate of geopolymerization reaction and lead to the reduction of reaction products.

(3) SEM and X-CT results show that the addition of EA can reduce the average pore diameter of SSGFC and improve the pore diameter distribution, thereby improving the compressive strength of SSGFC. When the EA content in the modified foam was 10 %, SSGFC exhibited the highest foam stability, maximum porosity and the most uniform pore diameter distribution. Specifically, by adding the modified foam with 10 % EA content, the 28d compressive strength of SSGFC increased by 21.4 %, and the water absorption and thermal conductivity decreased by 16.5 % and 31.3 %, respectively.

Based on the above conclusions, although it was observed that EA could delay the geological polymerization reaction, EA could still improve the mechanical strength of SSGFC by improving the pore diameter distribution. In addition, EA can also improve the water

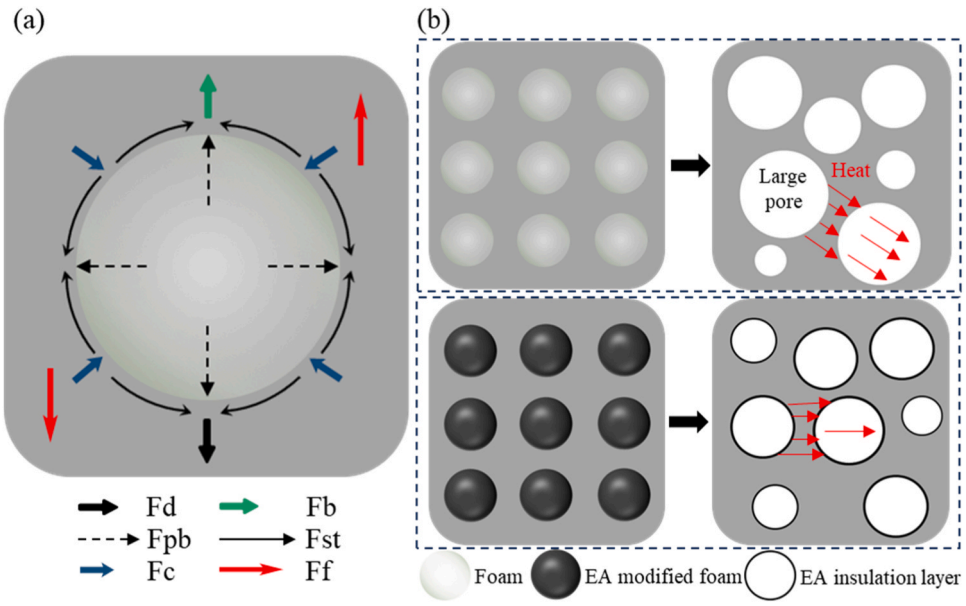

Fig. 15. The enhancement mechanism of EA on the thermal insulation performance of SSGFC, (a) Forces acted on single foam, (b) Heat transfer process.

absorption and thermal insulation properties of SSGFC. Therefore, EA is considered to have the potential to play a key role in SSGFC and promote the utilization of SS.

CRediT authorship contribution statement

Xuhui Liang: Investigation, Formal analysis. **Boyu Chen:** Investigation, Formal analysis. **Shi Xu:** Formal analysis, Conceptualization. **Shaopeng Wu:** Methodology, Conceptualization. **Zenggang Zhao:** Investigation, Formal analysis. **Dongyu Chen:** Investigation, Formal analysis. **Xinkui Yang:** Writing – original draft, Formal analysis, Conceptualization.

Declaration of Competing Interest

The authors declare that they have no known competing financial interests or personal relationships that could have appeared to influence the work reported in this paper.

Acknowledgements

This work was supported by National Natural Science Foundation of China (No. 52378461), Key R&D Program of Guangxi Province (No. AB21196061), Hubei Science and Technology Innovation Talent and Service Project (No. 2022EHB006), and Science and Technology Project of the Department of Transportation of Guangxi Autonomous Region (No. 2021-MS5-125).

Data availability

Data will be made available on request.

References

[1] X. Huang, J. Zhang, L. Zhang, Accelerated carbonation of steel slag: a review of methods, mechanisms and influencing factors, Constr. Build. Mater. 411 (2024) 134603.
[2] C. Yang, S. Wu, P. Cui, S. Amirkhanian, Z. Zhao, F. Wang, L. Zhang, M. Wei, X. Zhou, J. Xie, Performance characterization and enhancement mechanism of recycled asphalt mixtures involving high RAP content and steel slag, J. Clean. Prod. 336 (2022) 130484.
[3] P. Cui, S. Wu, Y. Xiao, R. Hu, T. Yang, Environmental performance and functional analysis of chip seals with recycled basic oxygen furnace slag as aggregate, J. Hazard. Mater. 405 (2021) 124441.
[4] E.O. Kurniati, F. Pederson, H.-J. Kim, Application of steel slags, ferronickel slags, and copper mining waste as construction materials: a review, Resour., Conserv. Recycl. 198 (2023) 107175.
[5] M. Kang, M.-C. Kang, A. Yonis, P. Vashistha, S. Pyo, Effect of steel slag on the mechanical properties and self-sensing capability of ultra-high performance concrete (UHPC), Dev. Built Environ. 17 (2024) 100342.
[6] X. Yu, J. Chu, S. Wu, K. Wang, Production of biocement using steel slag, Constr. Build. Mater. 383 (2023) 131365.
[7] H.L. Wang, J.S. Qian, J. Liu, X.L. Nan, S.Z. Qu, X.M. Li, Y. Liu, Wear resistance analysis of steel slag aggregates based on morphology characteristics, Constr. Build. Mater. 409 (2023) 133649.
[8] X. Li, H. Mehdizadeh, T.-C. Ling, Environmental, economic and engineering performances of aqueous carbonated steel slag powders as alternative material in cement pastes: influence of particle size, Sci. Total Environ. 903 (2023) 166210.
[9] G. Huang, M. Wang, Q. Liu, S. Zhao, H. Liu, F. Liu, L. Feng, J. Song, Simultaneous utilization of mine tailings and steel slag for producing geopolymers: alkali-hydrothermal activation, workability, strength, and hydration mechanism, Constr. Build. Mater. 414 (2024) 135029.
[10] J. Sun, S. Luo, Y. Wang, Q. Dong, Z. Zhang, Pre-treatment of steel slag and its applicability in asphalt mixtures for sustainable pavements, Chem. Eng. J. 476 (2023) 146802.
[11] Y. Xia, D. Shi, R. Zhao, K. Yu, M. Liu, H. Mei, L. Xu, Y. Zhao, L. Wang, J. Yan, Iron-rich industrial waste enhanced low-carbon radiation shielding functional composites, J. Clean. Prod. 449 (2024) 141649.
[12] D. Shi, Y. Xia, Y. Zhao, X. Ma, J. Wang, M. Liu, K. Yu, Evaluation of technical and gamma radiation shielding properties of sustainable ultra-high performance geopolymer concrete, Constr. Build. Mater. 436 (2024) 137003.
[13] D. Shi, Y. Xia, Y. Zhao, J. Wang, X. Ma, M. Liu, K. Yu, J. Zhang, W. Tian, Valorization of steel slag into sustainable high-performance radiation shielding concrete, J. Build. Eng. 91 (2024) 109650.
[14] G. Xiang, D. Song, H. Li, F.E. Jalal, H. Wang, Y. Zhou, Investigation on preparation and compressive strength model of steel slag foam concrete, J. Build. Eng. 72 (2023) 106548.
[15] Y.-L. Liu, C. Liu, L.-P. Qian, A.-G. Wang, D.-S. Sun, D. Guo, Foaming processes and properties of geopolymer foam concrete: effect of the activator, Constr. Build. Mater. 391 (2023) 131830.
[16] G. Kaplan, O. Yavuz Bayraktar, B. Bayrak, O. Celebi, B. Bodur, A. Oz, A.C. Aydin, Physico-mechanical, thermal insulation and resistance characteristics of diatomite and attapulgite based geopolymer foam concrete: effect of different curing regimes, Constr. Build. Mater. 373 (2023) 130850.
[17] A.M. Alnahhal, U.J. Alengaram, M.S.I. Ibrahim, S. Yusoff, H.S.C. Metselaar, P. Gabriela Johnson, Synthesis of ternary binders and sand-binder ratio on the mechanical and microstructural properties of geopolymer foamed concrete, Constr. Build. Mater. 349 (2022) 128682.
[18] W. Wang, Z. Zhong, X. Kang, X. Ma, Physico-mechanical properties and micromorphological characteristics of graphene oxide reinforced geopolymer foam concrete, J. Build. Eng. 72 (2023) 106732.
[19] A.M. Alnahhal, U.J. Alengaram, S. Yusoff, P. Darvish, K. Srinivas, M. Sumesh, Engineering performance of sustainable geopolymer foamed and non-foamed concretes, Constr. Build. Mater. 316 (2022) 125601.
[20] H. Xu, Y. Zou, G. Airey, H. Wang, H. Zhang, S. Wu, A. Chen, Wetting of bio-rejuvenator nanodroplets on bitumen: a molecular dynamics investigation, J. Clean. Prod. 444 (2024) 141140.

[21] X. Zhang, C. Qian, Z. Ma, F. Li, Study on preparation of supplementary cementitious material using microbial CO2 fixation of steel slag powder, Constr. Build. Mater. 326 (2022) 126864.
[22] H. Gao, H. Liao, X. Yao, F. Cheng, Insights into the reinforcing mechanism for CO2 atmosphere in the application process of steel slag ultra-fine powder, Constr. Build. Mater. 209 (2019) 437–444.
[23] Y. Shi, Q. Zhao, C. Xue, Y. Jia, W. Guo, Y. Zhang, Y. Qiu, Preparation and curing method of red mud-calcium carbide slag synergistically activated fly ash-ground granulated blast furnace slag based eco-friendly geopolymer, Cem. Concr. Compos. 139 (2023) 104999.
[24] S. Raj, K. Ramamurthy, Physical, hydrolytic, and mechanical stability of alkali-activated fly ash-slag foam concrete, Cem. Concr. Compos. 142 (2023) 105223.
[25] S. Yan, X. Ren, W. Wang, C. He, P. Xing, Preparation of eco-friendly porous ceramic with low thermal conductivity by high-temperature treatment of foamed solid waste based geopolymer with cenospheres, Constr. Build. Mater. 398 (2023) 131190.
[26] K. Dhasindrakrishna, K. Pasupathy, S. Ramakrishnan, J. Sanjayan, Progress, current thinking and challenges in geopolymer foam concrete technology, Cem. Concr. Compos. 116 (2021) 103886.
[27] Z. Zhang, J.L. Provis, A. Reid, H. Wang, Geopolymer foam concrete: an emerging material for sustainable construction, Constr. Build. Mater. 56 (2014) 113–127.
[28] Y. Li, J. Shen, H. Lin, Y. Li, Optimization design for alkali-activated slag-fly ash geopolymer concrete based on artificial intelligence considering compressive strength, cost, and carbon emission, J. Build. Eng. 75 (2023) 106929.
[29] B. Pratap, S. Mondal, B. Hanumantha Rao, NaOH molarity influence on mechanical and durability properties of geopolymer concrete made with fly ash and phosphogypsum, Structures 56 (2023) 105035.
[30] L. Su, G. Fu, B. Liang, Q. Sun, X. Zhang, Mechanical properties and microstructure evaluation of fly ash - slag geopolymer foaming materials, Ceram. Int. 48 (13) (2022) 18224–18237.
[31] X. Zhang, X. Zhang, M. Ma, Y. Sun, C. Ma, Rapid performance optimization strategy of MK-FA-GBFS based geopolymer foam heavy-metal adsorbent, Constr. Build. Mater. 394 (2023) 132161.
[32] Y. Hao, G. Yang, K. Liang, Development of fly ash and slag based high-strength alkali-activated foam concrete, Cem. Concr. Compos. 128 (2022) 104447.
[33] A.I. Badanoiu, T.H.A. Al Saadi, S. Stoleriu, G. Voicu, Preparation and characterization of foamed geopolymers from waste glass and red mud, Constr. Build. Mater. 84 (2015) 284–293.
[34] Z. Shao, B. Ma, J. Wang, Q. Cai, J. Jiang, B. Qian, G. Cheng, Y. Hu, F. Ma, J. Sun, L. Wang, The influence of ZSM-5 waste on the properties of fly ash-based foamed geopolymer, J. Clean. Prod. 355 (2022) 131800.
[35] G. Murali, Recent research in mechanical properties of geopolymer-based ultra-high-performance concrete: a review, Def. Technol. 32 (2024) 67–88.
[36] H. Unis Ahmed, A.S. Mohammed, A.A. Mohammed, Fresh and mechanical performances of recycled plastic aggregate geopolymer concrete modified with Nano-silica: experimental and computational investigation, Constr. Build. Mater. 394 (2023) 132266.
[37] D. Polat, M. Güden, Processing and characterization of geopolymer and sintered geopolymer foams of waste glass powders, Constr. Build. Mater. 300 (2021) 124259.
[38] Z. Shao, J. Wang, Y. Jiang, J. Zang, T. Wu, F. Ma, B. Qian, L. Wang, Y. Hu, B. Ma, The performance of micropore-foamed geopolymers produced from industrial wastes, Constr. Build. Mater. 304 (2021) 124636.
[39] S. Yan, F. Zhang, J. Kong, B. Wang, H. Li, Y. Yang, P. Xing, Mechanical properties of geopolymer composite foams reinforced with carbon nanofibers via modified hydrogen peroxide method, Mater. Chem. Phys. 253 (2020) 123258.
[40] W. Feng, Y. Jin, D. Zheng, Y. Fang, Z. Dong, H. Cui, Study of triethanolamine on regulating early strength of fly ash-based chemically foamed geopolymer, Cem. Concr. Res. 162 (2022) 107005.
[41] Y. Zhang, Y. Jiang, T.-C. Ling, Use of CO2 as a controlled foam stabilizer to enhance pore structure and properties of foamed concrete, Cem. Concr. Compos. 145 (2024) 105356.
[42] C. Dong, N. Shao, F. Yan, R. Ji, X. Wei, Z. Zhang, A novel integration strategy for the foaming and hydrophobization of geopolymer foams, Cem. Concr. Res. 160 (2022) 106919.
[43] J. Wang, X. Li, Y. Hu, Y. Li, P. Hu, Y. Zhao, Physical and high temperature properties of basalt fiber-reinforced geopolymer foam with hollow microspheres, Constr. Build. Mater. 411 (2024) 134698.
[44] Z. Wang, T. Xia, J. Xu, Y. Li, M. Wang, Effect of polyurethane addition on the dynamic mechanical properties of cement emulsified asphalt, Constr. Build. Mater. 401 (2023) 132693.
[45] C. Ma, Y. Wu, J. Shi, S. Song, F. Xia, J. Liu, H. Zhou, B. Dong, Y. Du, Preparation and characterization of a novel magnesium phosphate cement-based emulsified asphalt mortar, Ceram. Int. 49 (13) (2023) 21422–21432.
[46] S. Jiang, J. Li, Z. Zhang, H. Wu, G. Liu, Factors influencing the performance of cement emulsified asphalt mortar – a review, Constr. Build. Mater. 279 (2021) 122479.
[47] A.H. Saesaei, A. Sahaf, S. Najjar, M.R.M. Aliha, Laboratory investigation on the fracture toughness (Mode I) and durability properties of eco-friendly cement emulsified asphalt mortar (CRTS II) exposed to acid attack, Case Stud. Constr. Mater. 20 (2024) e02719.
[48] Z. Tong, Z. Wang, X. Wang, Y. Ma, H. Guo, C. Liu, Characterization of hydration and dry shrinkage behavior of cement emulsified asphalt composites using deep learning, Constr. Build. Mater. 274 (2021) 121898.
[49] S. Najjar, A. Mohammadzadeh Moghaddam, A. Sahaf, M.R.M. Aliha, Low temperature fracture resistance of cement emulsified asphalt mortar under mixed mode I/III loading, Theor. Appl. Fract. Mech. 110 (2020) 102800.
[50] Z. Wang, X. Shu, T. Rutherford, B. Huang, D. Clarke, Effects of asphalt emulsion on properties of fresh cement emulsified asphalt mortar, Constr. Build. Mater. 75 (2015) 25–30.
[51] Y. Li, H. Sun, X. He, Y. Tan, Fatigue damage and creep characteristics of cement emulsified asphalt composite binder, Constr. Build. Mater. 234 (2020) 117416.
[52] S. Liu, Y. Tan, Mechanical properties and water resistance study of basic magnesium sulfate cement-emulsified asphalt composite materials, Constr. Build. Mater. 426 (2024) 136196.
[53] M.N. Razali, N. Mohd Ramli, K.N. Mohd Zuhan, M. Musa, A. Hamid Nour, Coating and insulation effect using emulsified modification bitumen, Constr. Build. Mater. 260 (2020) 119764.
[54] X. Jiang, Y. Zhang, Y. Zhang, J. Ma, R. Xiao, F. Guo, Y. Bai, B. Huang, Influence of size effect on the properties of slag and waste glass-based geopolymer paste, J. Clean. Prod. 383 (2023) 135428.
[55] Y. Xia, D. Shi, J. Wang, Y. Zhao, K. Yu, Y. Liu, H. Cui, L. Wang, Value-added recycling of cathode ray tube funnel glass into high-performance radiation shielding concrete, Resour., Conserv. Recycl. 199 (2023) 107252.
[56] X. Gu, S. Wang, J. Liu, H. Wang, X. Xu, Q. Wang, Z. Zhu, Effect of hydroxypropyl methyl cellulose (HPMC) as foam stabilizer on the workability and pore structure of iron tailings sand autoclaved aerated concrete, Constr. Build. Mater. 376 (2023) 130979.
[57] Ministry of Housing and Urban-Rural Development of the People's Republic of China. Technical specification for foamed mixture lightweight soil filling engineering: CJJ/T 177-2012, 2012.
[58] H. Zhang, S. Yao, J. Wang, C. Hou, X. Guan, D. Zou, A novel CO2 foaming agent for the preparation of foamed sulfoaluminate cement material: application to coal mine filling, J. Build. Eng. 62 (2022) 105353.
[59] C. Zhang, J. Yang, J. Fu, S. Wang, J. Yin, Y. Xie, L. Li, Cement based eco-grouting composite for pre-reinforcement of shallow underground excavation in vegetation protection area, Tunn. Undergr. Space Technol. 118 (2021) 104188.
[60] X. Pang, J. Singh, W. Cuello Jimenez, Characterizing gas bubble size distribution of laboratory foamed cement using X-ray micro-CT, Constr. Build. Mater. 167 (2018) 243–252.
[61] M. Li, H. Tan, X. He, S. Jian, G. Li, J. Zhang, X. Deng, X. Lin, Enhancement in compressive strength of foamed concrete by ultra-fine slag, Cem. Concr. Compos. 138 (2023) 104954.
[62] Ministry of Housing and Urban-Rural Development of the People's Republic of China. Foamed concrete: JG/T 266-2011, 2011.
[63] T. Guo, M. Qiao, X. Shu, L. Dong, G. Shan, X. Liu, Y. Guo, Q. Ran, Characteristic analysis of air bubbles on the rheological properties of cement mortar, Constr. Build. Mater. 316 (2022) 125812.
[64] S. Yan, D. Pan, J. Dan, J. Wang, Y. Yu, Calcium carbide residue and Glauber's salt as composite activators for fly ash-based geopolymer, Cem. Concr. Compos. 140 (2023) 105081.
[65] H. Zhang, G. Zhou, Q. Zhang, S. Zhang, Y. Pei, X. Kong, M. Zhang, F. Skoczylas, Effects of emulsified asphalt on the rheological behaviors of magnesium phosphate cement, Constr. Build. Mater. 403 (2023) 133205.
[66] G. Li, H. Tan, X. He, J. Zhang, X. Deng, Z. Zheng, Y. Guo, The influence of wet ground fly ash on the performance of foamed concrete, Constr. Build. Mater. 304 (2021) 124676.
[67] Z.Y. Qu, Q. Yu, Y.D. Ji, F. Gauvin, I.K. Voets, Mitigating shrinkage of alkali activated slag with biofilm, Cem. Concr. Res. 138 (2020) 106234.
[68] L. Jiang, Z. Wang, X. Gao, M. Cui, Q. Yang, J. Qin, Effect of nanoparticles and surfactants on properties and microstructures of foam and foamed concrete, Constr. Build. Mater. 411 (2024) 134444.
[69] D. Chen, M. Chen, Y. Zhang, X. Yang, J. Zhang, Y. Zhao, Y. Wu, Development of an environmental foamed concrete incorporating recycled cement concrete powder with carbonation, Constr. Build. Mater. 422 (2024) 135833.
[70] W. She, Y. Du, C. Miao, J. Liu, G. Zhao, J. Jiang, Y. Zhang, Application of organic- and nanoparticle-modified foams in foamed concrete: reinforcement and stabilization mechanisms, Cem. Concr. Res. 106 (2018) 12–22.